https://doi.org/10.5194/egusphere-2024-676
Preprint. Discussion started: 18 March 2024

El Niño Enhances Snowline Rise and Ice Loss on the World's Largest Tropical Ice Cap

Kara A. Lamantia[1,2], Laura J. Larocca[3], Lonnie G. Thompson[1,2], Bryan G. Mark[1,4]

[1] Byrd Polar and Climate Research Center, Ohio State University, Columbus, OH, USA
[2] School of Earth Sciences, Ohio State University, Columbus, OH, USA
[3] School of Ocean Futures, Arizona State University, Tempe, AZ, USA
[4] Department of Geography, Ohio State University, Columbus, OH, USA

Correspondence to: Kara A. Lamantia (lamantia.31.@osu.edu)

Abstract. Tropical glaciers are essential water resources in the central Andes as vital water resources and crucial climate indicators, currently undergoing rapid retreat. However, understanding their vulnerability to the combined effects of persistent warming, short-term climate phenomena, and interannual fluctuations remains limited. Here we automate mapping of key mass balance parameters on the Quelccaya Ice Cap (QIC), the world's largest tropical ice cap. Using Landsat's near-infrared (NIR) band, we analyze snow cover area (SCA) and total area (TA) and calculate the Accumulation Area Ratio (AAR) and Equilibrium Line Altitude (ELA) over nearly 40 years (1985-2023). Between 1985 and 2022, the QIC lost ~46% and ~34% of its SCA and TA, respectively. We show that the QIC's loss in SCA and rise in ELA are exacerbated by El Niño events, which are strongly correlated to the preceding wet season's Ocean Niño Index (ONI). We observe lower levels of correlation to more recent El Niño events as anthropogenic climatic impacts overwhelm the natural forcing and continue to exacerbate loss at the QIC.

1 Introduction

Tropical glaciers are known to be especially sensitive to climate shifts (Kaser & Osmaston, 2002) and their accelerated decline has been well documented in recent decades (Bradley et al., 2006; Braun et al., 2019; Hanshaw & Bookhagen, 2014a; Hugonnet et al., 2021; Pepin, 2015; Seehaus et al., 2020; Thompson et al., 2011, 2021; Vuille et al., 2015). In the low latitudes and southern Andes, glaciers are projected to lose ~76-99% and ~49-74% of their 2015 mass, respectively, depending on the emissions scenario (Rounce et al., 2023). The freezing level height in the tropics is affected on an interannual basis by El Niño Southern Oscillation (ENSO) variations and follows the Multivariate ENSO Index (MEI) on a year-to-year basis (Bradley et al., 2009; Favier et al., 2004; Thompson, 2000; Vuille et al., 2000). The decline of the Quelccaya Ice Cap (QIC; the world's largest tropical ice cap; Fig. 1), located in the Cordillera Vilcanota (CV) range in the outer tropical region of the Andes, is one such concern with worst case (RCP8.5) projections suggesting its disappearance as early as 2050 (Yarleque et al., 2018). Contemporary changes in the QIC's outlet glaciers have been monitored frequently (Brecher & Thompson, 1993) with modern rates exceeding those reconstructed from Holocene moraines (Mark et al., 2002). Further evidence of the QIC has recently

https://doi.org/10.5194/egusphere-2024-676
Preprint. Discussion started: 18 March 2024

been placed within a longer-term context using radiocarbon-dated plant remains from the ice margin suggesting that the ice cap's present-day magnitude of retreat has not occurred since at least 7,000 years ago (Lamantia et al., 2023). In addition, the QIC's high-resolution ice-core records have proven invaluable for understanding of past climatic and environmental variability in the region (Thompson, 2000; Thompson et al., 1985, 2013, 2017, 2021). Thus, the ongoing loss of tropical glaciers will not only impact local communities that depend on glacial meltwater but has implications for the preservation of long-term climate records, essential for assessing the rate and magnitude of current changes (Thompson et al., 2021).

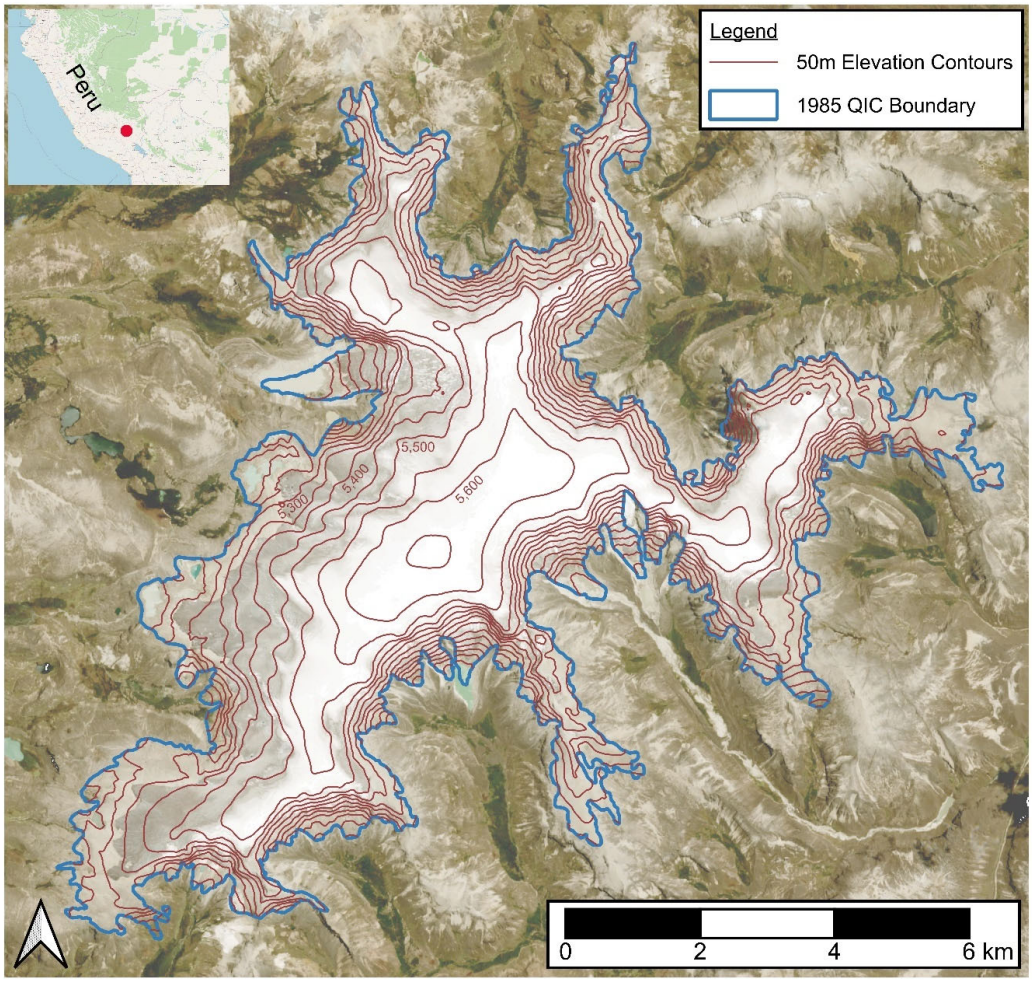

Figure 1: Aerial view of the Quelccaya Ice Cap (13°56'S; 70°50'W) from October 11, 2023. The summit of the QIC reaches 5,670 m a.s.l with a handful of outlet glaciers to the west and a steep-sided eastern portion. Base Imagery was obtained from Planet Labs Dove Satellite with 3-meter resolution and inset (top left) was obtained from the OpenStreetMap database (© OpenStreetMap contributors 2023. Distributed under the Open Data Commons Open Database License (ODbL) v1.0.)

https://doi.org/10.5194/egusphere-2024-676
Preprint. Discussion started: 18 March 2024

In the tropics, there is no seasonal snow cover beyond the glacierized area that would provide an additional buffer to the ice cap's decline (Vuille et al., 2018). The southern wet outer tropics are climatically controlled by fluctuations in the Intertropical Convergence Zone (ITCZ) and glaciers such as the QIC have enhanced temperature sensitivity relative to those in the dry outer tropics (Veettil et al., 2017). There has been no significant change in precipitation around the QIC over the last fifty years, with 10% of stations in the CV recording only a slight decrease in rainfall (Casimiro et al., 2013) but ice core records from the QIC core reveal the net accumulation in the region has been above average for the last century (Thompson L.G., 2017). The average temperature has increased by ~0.09°C per decade over the last sixty years with the summer months recording a higher magnitude increase in maximum temperature (Casimiro et al., 2013) and ice cores recording documenting the accelerating enrichment (Thompson L.G, 2017). Nearby mountain ranges such as the Cordillera Blanca and Real have experienced an increase in the freezing level height (FLH) by 160 m over the last five and a half decades with implications for where snow can survive and accumulate (Bradley et al., 2009; Schauwecker et al., 2014; Seehaus et al., 2020). High-resolution ice core records show that the QIC is an excellent recorder of the El Niño and La Niña events that create elevated sea surface temperatures (SSTs) in the Eastern Pacific Ocean, recording years of strong El Niño events with isotopically enriched $\delta^{18}O$ (Thompson et al., 2011, 2017). Alongside these ice core records, the QIC's contemporary and past margin has been monitored and reconstructed, but it has yet to be evaluated for ice loss and response to these short-term climate phenomena that may play a role in its current decline. Thus, the QIC is an ideal setting to assess the combined effects of sustained warming and short-term climate variations, such as ENSO, on tropical glacier vulnerability.

Since routine ground-based measurements in a remote location such as south-central Peru are difficult to maintain, using satellite imagery to estimate the Equilibrium Line Altitude (ELA) has become a viable solution. Previous studies have shown that the end of dry season (September) location of the snowline altitude (SLA) can act as a proxy for the ELA and ultimately be used to infer the mass balance of a glacier or ice cap (Fang et al., 2011; Hu et al., 2020; Liu et al., 2021; Racoviteanu et al., 2019). Here, we use a suite of imagery spanning 1985 to 2023 to assess the QIC at the end of the dry season through a cloud-based analysis of satellite imagery. We automate not only the detection of the snow-covered area (SCA) and total area (TA), but also the calculation of the accumulation area ratio (AAR), the median elevation of the SCA, and the SLA as a proxy for the ELA. Changes to the ELA, SCA, and AAR are analyzed alongside ERA5 – Land Reanalysis Climate Data from the European Centre for Medium Weather Range Weather Forecast (ECMWF) including total precipitation and surface temperature as well as multiple ENSO Indices including the MEI, the Ocean Niño Index (ONI), and the Southern Oscillation Index (SOI). We additionally focus on the most recent El Niño events (1998, 2016, & 2023) and the QIC's response to these short-term climate anomalies.

https://doi.org/10.5194/egusphere-2024-676
Preprint. Discussion started: 18 March 2024

2 Methods

2.1 Current Analysis Techniques

Recent advances in image analysis have included the automation of snowline detection as often manual tracing is limited to higher quality imagery to determine snow versus ice presence. Typically, a suite of images, often from Landsat satellites are paired with one or more Digital Elevation Models (DEMs) and a glacier outline from the beginning of the temporal scale of interest (Li et al., 2022). From there, a variety of thresholds are evaluated and set for the area of interest with the SLA extracted from automated calculations to be used as the ELA (Racoviteanu et al., 2019) or manual tracing of outputs (Liu et al., 2021). There are challenges in this process including adjusting surface reflectance from the topography, patchy snow cover on a glacier, and highly variable atmospheric conditions that require the algorithm to be adjusted to the location of interest (Racoviteanu et al., 2019). Previous studies have included a handful of techniques including satellite imagery analysis and spectral mixing from the Landsat short-wave infrared (SWIR) and near-infrared (NIR) bands (Klein & Isacks, 1999), as well as satellite imagery band ratios, hillshade shadow removal, and manual editing (Hanshaw & Bookhagen, 2014a).

2.2 Data Collection

To automate the SCA detection and ELA calculation, the following data inputs were required: an annual satellite image, a DEM, and the 1985 outline of the QIC. Using the Google Earth Engine platform (GEE) we select annual Landsat images as close as possible to September 1st with clear visibility of the QIC from 1985 to 2023 (Table S1). September 1st marks the end of the dry season in the CV, enabling analysis of the ice cap without extraneous snowfall around the perimeter. Imagery from each year was manually inspected to ensure no recent snowfall events occurred and were not used if recent snowfall was evident. Sentinel-2 imagery was used in 2023, due to a lack of cloudless images from Landsat 8/9. As one of our aims was to analyze the 2023 El Niño event, a separate script was adapted for the higher resolution and alternate detail of Sentinel-2 processing. We note that 2023 results are not included in our initial analysis of QIC's ELA change as it is part of an incomplete El Niño event. No imagery was collected for the years 1987, 1994, 2002, and 2012 due to high cloud cover. DEM usage accounted for changes in ice elevation over time and any down-wasting of the QIC, and initially the NASADEM, created from the Shuttle Radar Topography Missions (SRTM), was implemented from 1985 to 2005. Post 2005, the COP30 DEM, released in 2010, was implemented following an assessment of surface difference in both DEMs between 2005 to 2015. Additionally, throughout the two largest El Niño events (1997-1999 & 2015-2017) 16 and 18 images, respectively, were collected to assess short-term change and response of the QIC to El Niño.

2.3 Satellite Analysis for Snow Cover Area

To begin, the least cloudy image from the year is clipped to the region of interest (ROI), the delineated QIC boundary (Step 1; Fig. S1). Pre-processing of each image includes calculating the illumination condition, which for the detection of the same features under different sunlight conditions (Step 2; Martín-Ortega et al., 2020). We use the Minnaert Correction (Ge et al.,

https://doi.org/10.5194/egusphere-2024-676
Preprint. Discussion started: 18 March 2024

2008), which assumes the reflectance of a surface is proportional to the cosine of the angle of incidence. Both are used to topographically correct for variability of observed reflectance and apply such to the selected annual image (Step 3; Ge et al., 2008). The QIC is an excellent case study for this method as the low-sloping topography does not create as many shadows as a steep mountain glacier. To delineate the snow cover area (SCA), the NIR band is assessed with an image segmentation algorithm, the OTSU method (Gaddam et al., 2022). The NIR band records a bimodal frequency histogram of snow and ice and the OTSU method is designed to automatically detect the threshold to separate snow from ice (Step 4; Fig. S2). Once calculated, it is applied to the NIR band to create a binary mask of snow and ice (Step 4). The annual image and DEM are clipped to the snow mask creating the SCA, and the DEM data is extracted (Step 5) and the SCA and median elevation of the SCA are calculated. SCAs are exported to shapefiles and the DEM data is exported as a histogram in 50-meter elevation bins (Step 6).

2.3 Calculation of Total Area, AAR, and ELA, and Uncertainty

As the SLA is a proxy for the ELA, we will use the term ELA from this point forward. In pursuit of the ELA, we calculate the Accumulation Area Ratio (AAR). The AAR is defined as: AAR = Ac/(Ac +Ab) where Ac is the accumulation area and Ac + Ab is the total area (TA) (Meier, 1962). In this case, Ac is the SCA and Ac+Ab is the TA (both ice & snow). To calculate the TA, we automate the calculation of the Normalized Difference Snow Index (NDSI), which leverages the reflectance of snow and ice in the green and SWIR spectra compared to other land cover types. The NDSI is calculated by the following equation: $NDSI = (\rho_G - \rho_{SWIR})/(\rho_G + \rho_{SWIR})$, where ρ_G and ρ_{SWIR} are the reflectance of the green and shortwave infrared bands, respectively (Dozier, 1989; Hall & Riggs, 2007). We use the same OTSU thresholding method to calculate the NDSI threshold, typically set around 0.4 (Dozier, 1989; Hall & Riggs, 2007; Sankey et al., 2015). The number of snow- and ice-covered pixels is multiplied by the appropriate pixel resolution to obtain the TA. By applying the threshold to each image, we obtain a binary image of snow/ice versus neither and use this to calculate the TA (Step 7). The AAR is calculated by dividing the SCA by the TA (Step 8). We calculate the ELA using the DEM and the AAR by calculating the 1 – AAR percentile of all elevations in the TA (Step 9: Fig. S3). For example, if the AAR is 0.8, we assume the ELA is located at the 20th percentile of elevations in the TA. In summary, for each image analyzed, we obtain the SCA, the median elevation, the TA, the AAR, and the ELA. Calculated results are robust with seven manual digitizations of the ELA resulting in a SCA within ±3% of the automated calculation. Other studies have shown manual and automated detection of snowline produces similar and albeit low level of error (Hanshaw & Bookhagen, 2014b).

2.4 Renanalysis Data and ENSO Correlation

To observe SCA and ELA alongside climatic variables we use daily and monthly averaged data from the ERA5 – Land Reanalysis Climate Data from the European Centre for Medium Weather Range Weather Forecast (ECMWF) including total precipitation and surface temperature. Initially, we divided the data into wet (October to April) and dry (May to September) seasons based on precipitation records and past literature (Kaser & Osmaston, 2002; Veettil et al., 2017). To observe change

https://doi.org/10.5194/egusphere-2024-676
Preprint. Discussion started: 18 March 2024

at the QIC over time we calculate the average precipitation and temperature in five-year intervals, and the number of average days above and below freezing for each season from 1985 to 2023. To analyze the QIC's interannual response to climatic anomalies we paired detrended ELA, SCA, and median elevation with the MEI, SOI, and ONI indices for correlation. As such, the variables for each year were correlated with the preceding months' indices for one year before the annual September observation date.

3 Results

3.1 Ice Loss and Multi-Decadal Climate Trends

Over the observation period (1985 and 2022), the QIC lost ~34% of its TA and ~46% of its SCA (1985: TA=~59.6 km^2, SCA=~46.8 km^2; 2022: TA=~39.6 km^2, SCA=~25.3 km^2 (Table S2). This SCA loss is concurrent with a retreat of the TA to higher elevations (Fig. 2). We observe a 168 m and 84 m rise of the ELA and median elevation of the SCA, respectively. In 1985, 90% of the SCA existed above 5,250 m a.s.l., and by 2022, 90% of the SCA shifted to elevations above 5,350 m a.s.l. On average, linear regression models suggest a loss of 0.39±0.09 km^2 yr^{-1} (R^2=0.36, p<0.001) in the QIC's SCA; an average loss of 0.48±0.03 km^2 yr^{-1} (R^2=0.89, p<0.001) in the QIC's TA; and an average rise of 2.96±0.75 m yr^{-1} (R^2=0.32, p<0.001) in the QIC's ELA. However, removal of the three El Niño influenced years (1998, 2016, and 2023) indicate slower average losses in QIC's SCA and TA, and a slower average rise in QIC's ELA: -0.36±0.07 km^2 yr^{-1} (R^2=0.50, p<0.001); -0.47±0.03 km^2 yr^{-1} (R^2=0.89, p<0.001); and +2.72±0.59 m yr^{-1} (R^2=0.42, p<0.001), respectively (Table S3). The QIC's average AAR (minus El Niño years) is 0.74 throughout the study period, with 1998, 2016, and 2023 (0.30, 0.51, & 0.52), as the exceptions. Our measured variables show significant correlation to each other. For example, we find a strong positive correlation between the median elevation and the ELA (0.98), a strong negative correlation between the ELA and the SCA (-0.98) and a strong positive correlation between the SCA and AAR (0.84, Table S4).

The QIC's daily and monthly variations recorded by the QIC summit and bottom margin weather stations from Bradley et al., (2009) are well correlated with the ERA5 surface temperature dataset, which was analyzed to determine changes in meteorological variables through the observation period. Analysis of the ERA5 surface temperature data records ~46% of the wet season (October – April) and ~11% of the dry season (May – September) with mean daily temperatures above 0°C. The average temperature of the first five and last five years show an increase of 0.59°C in the wet season and 1.24°C in the dry season. Similarly, the number of days above 0°C rose from 32% to 50% in the wet season and from 5% to 17% in the dry season over the first five and last five years. These results are consistent with previous studies discussing a 0.1°C/decade rise in the freezing line in the tropics near the QIC (Bradley et al., 2009; Vuille et al., 2008). We observe an unchanging trend in precipitation in both the wet and dry seasons with 73% of the precipitation occurring during the wet season.

https://doi.org/10.5194/egusphere-2024-676
Preprint. Discussion started: 18 March 2024

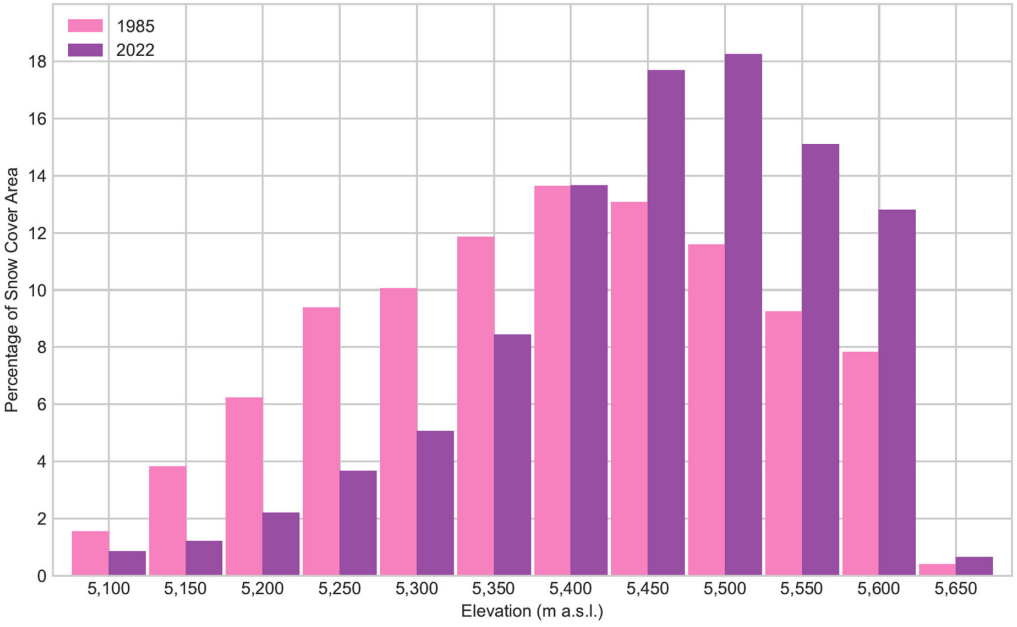

Figure 2: Percentage of snow cover area (SCA) in 50 meter elevation bins, demonstrating the shift to higher elevations.

3.2 QIC Response to Short-Term Climate Phenomena

El Niño events coincide with a large decrease in the QIC's SCA. We observe a 63% loss in SCA from 1997 to 1998 and a 40% loss from 2015 to 2016. In 1999, a rebound of the SCA is observed back to 1997 conditions however, in 2017 the SCA only reaches about 70% of its 2015 value following the 2016 El Niño (Fig. 3). A full rebound in the SCA is not observed until two years following the event, in 2018. To better determine the patterns during the El Niño events, high frequency sampling was conducted around the complete El Niño events, consisting of 16 and 18 images collected between 1997 – 1999 and 2015 – 2017, respectively. In both cases, the lowest SCA during the El Niño is observed in the annual September measurement, with a steady decline occurring from the prior year's September measurement. The 1997 to 1998 AAR drops from 0.75 to 0.30 and 2015 to 2016 from 0.78 to 0.51. During these El Niño events noticeable spikes are recorded in ERA5 temperature records while precipitation patterns and magnitude remain largely unchanged. If we fit the linear regression model with El Niño years as a binary predictor, the coefficients for the ELA and SCA (R^2=0.67, $p<0.001$; & R^2=0.67, $p<0.001$) improve with statistically significant values. However, the TA coefficient improves (R^2=0.90, $p=0.73$) but without statistically significant values. Similarly, an analysis of variance testing (ANOVA) with a post hoc test records a significant difference in the mean SCA and ELA from El Niño to neutral conditions and in the AAR El Niño to neutral and El Niño to La Niña (Fig S1). The TA does not record any significant different within El Niño, La Niña, to neutral conditions (Table S5). As the 2023 measurements occur

https://doi.org/10.5194/egusphere-2024-676
Preprint. Discussion started: 18 March 2024

during an ongoing El Niño event, we initially complied data from 1985 to 2022 and report the 2023 data as an additional insight to the effects of El Niño events on the QIC. The QIC's SCA observed during the onset of the 2023 El Niño is ~19.0 km^2, a 25% loss compared to that of 2022. The 2023 AAR is calculated at 0.52, well below the average. From 2022 to 2023, we observe a 31 m and 28 m rise of the ELA and median elevation with 90% of the SCA existing over 5,400 m a.s.l. as opposed to 5,350 m a.sl. in 2022. Overall, between 1985 to 2023, we observe a 60% decline in the QIC's SCA in just under 40 years (Fig. 4). We intend to continue to monitor the QIC to determine the continued effects of the El Niño event and any possible rebound that could occur in 2024.

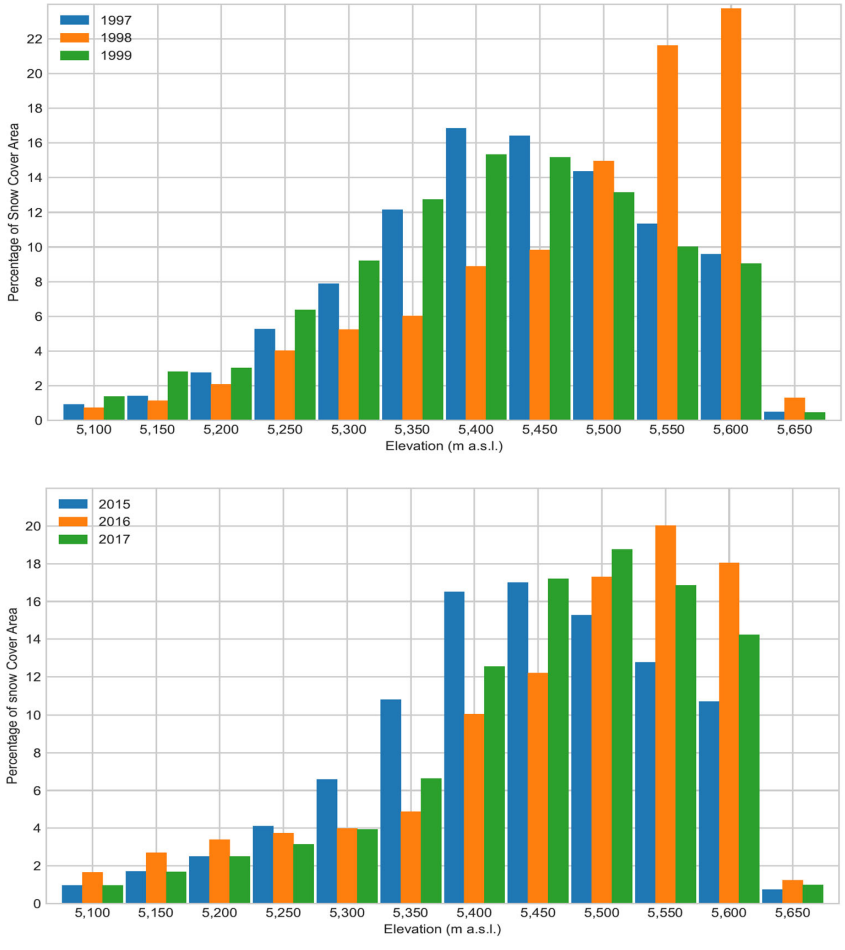

Figure 3: Percentage of snow cover displaying loss and rebound of the SCA during the 1998 El Niño event (top) and incomplete recovery following the 2016 El Niño event (bottom).

https://doi.org/10.5194/egusphere-2024-676
Preprint. Discussion started: 18 March 2024

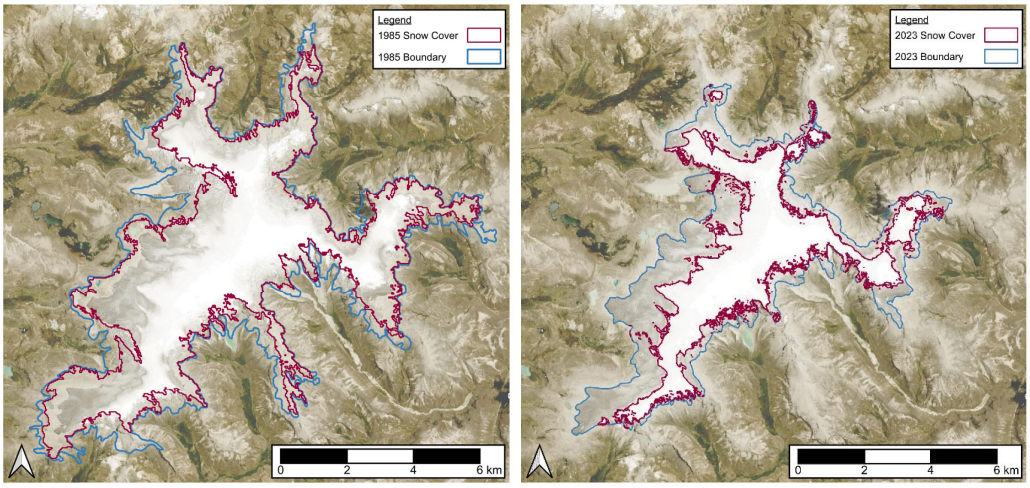

Figure 4: Decrease in the QIC's SCA (pink) and TA (blue) at the end of the dry season from 1985 (left) to 2023 (right). Base Imagery obtained from Planet Labs Dove Satellite with 3-meter resolution.

ENSO indices were most strongly correlated with the QIC's ELA, SCA, and median elevation as they best represent the changing ice distribution and mass. We evaluated all three ENSO indices but have chosen to discuss the ONI index as it presented the clearest patterns between index and the assessed QIC variables (Table S6). The ONI index is measured as sea surface temperature (SST) anomalies in the Niño 3.4 zone (5˚N - 5˚S & 120˚W – 170˚W) and is most used to define El Niño and La Niño events. The ONI index is most strongly correlated to the median elevation (Table 1) with a Pearson coefficient from the preceding April back through the previous September ranging from 0.489 to 0.644 ($P<0.05$). The ELA and median elevation follow a similar pattern with the prior wet season (March through September) recording the highest correlations (0.517 to 0.644). The SCA shows a similar pattern through a negative correlation from the prior wet season (-0.555 to -0.641).

https://doi.org/10.5194/egusphere-2024-676
Preprint. Discussion started: 18 March 2024

Preceding Month	*ELA*	*SCA*	*Med Elev*
September	***0.608***	***-0.641***	***0.644***
October	***0.555***	***-0.614***	***0.616***
November	***0.551***	***-0.609***	***0.612***
December	***0.549***	***-0.607***	***0.611***
January	***0.547***	***-0.599***	***0.602***
February	***0.548***	***-0.593***	***0.596***
March	***0.517***	***-0.555***	***0.562***
April	***0.441***	***-0.475***	***0.489***
May	0.271	-0.288	0.311
June	0.012	-0.005	0.034
July	-0.148	-0.176	-0.142
August	-0.213	0.245	-0.211

Table 1: Zero-order correlations (*r*) for QIC variables (ELA, SCA, and Median Elevation (Med Elev)) and the ONI Index. Coefficient with statistically significant p-values (<0.05) are indicated in bold italics.

4 Discussion

4.1 QIC Response to Short-Term Climate Variability

During El Niño events, Peru records higher precipitation along the northern coast, the Amazon, and the Andes (Lagos et al., 2008). To be considered an El Niño event, the SST anomalies must be high for at least four consecutive months (Lagos et al., 2008), and it is likely that these longer term SST anomalies have a greater influence on the SCA than singular precipitation events, of which no correlation is observed. We see evidence of these El Niño events in 1998 and 2016 impacting the SCA and TA (Fig. 5). These perturbations are outliers from the observed decline and are evident in QIC shallow ice cores which display a 'smoothed' $\delta^{18}O$ signal during the El Niño instead of the usual high resolution variability (Thompson et al., 2017). Regression analysis completed with and without El Niño events record differing slope coefficients, indicating these events are enhancing the QIC ice loss. As noted in the results, the SCA rebound from the 2016 El Niño did not fully occur until two years later, unlike in 1999. This suggest the magnitude of La Niña events are an additional factor as 1999 was one of the strongest within the observation period, along with 1989 and 2011. As these conditions persist, ELA and ONI index correlation declines from 0.65 to 0.34 from the 1998 to 2016 El Niño. The linear regression model with the El Niño binary predictor records a strong and significant relationship between TA and year, but variance testing indicates the presence of El Niño years provided a stronger impact to the SCA, AAR, and ELA than the TA (Fig. S4, Table S5). Multiple regression analyses between the ELA and ONI index record an r-squared of 0.43 ($p=0.1$) from 1997 to 1999 and an r-squared of 0.12 ($p<0.05$) from 2015 to 2017. This suggests that anthropogenic warming is overtaking natural climatic variability as the dominant control on the long-term presence of the QIC. The decrease in the percent of days at or below freezing during the wet season, will only exacerbate the decline. In addition, a recent study has indicated the expectation of faster onsets and slower decline for future El Niños (Lopez

https://doi.org/10.5194/egusphere-2024-676
Preprint. Discussion started: 18 March 2024

et al., 2022), and considering the current state of the QIC and the ongoing El Niño, a slow decline after the current event will only delay recovery in the SCA and continue to intensify its decline.

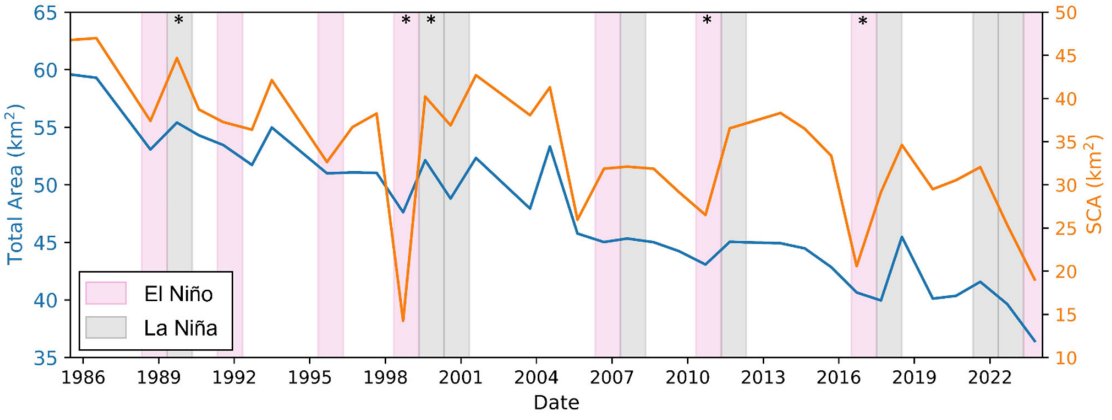

Figure 5: Decline of QIC's TA and SCA over the observational period (1985-2023). Timing of El Niño and La Niña events coincide more readily with SCA than TA changes. Strongest events are denoted with stars (*).

4.2 Equilibrium State of the QIC

Glaciers in other locations such as the New Zealand Alps and the European Alps are considered in steady state with AARs around 0.6 (Benn & Lehmkuhl, 2000), but tropical glaciers require an AAR of ~0.8 (Kaser & Osmaston, 2002). Discounting El Niño years (1998, 2016, & 2023), the QIC average AAR is 0.74, indicating it is out of equilibrium with the pace of ongoing changing climate. The ice cap is noticeably out of equilibrium during the observed El Niño events with AARs of 0.30, 0.51, and 0.52. These are far lower values than required for even high latitude glacier, and far below the average for the QIC. The SCA changes more dramatically on a year-to-year basis than the TA (Fig. 5), but the quick rebound of the AAR indicates rapid response to short-term climate variability and more recent decadal scale changes (Zekollari et al., 2020). The median elevation of the entire QIC was recorded rising 1.59 m per decade from 1975 to 2010 (Taylor et al., 2022), slightly less than this estimate although the temporal scale observed was different. The QIC is likely responding to climate drivers within a few decades from the present, including the almost immediate response to El Niño events (Thompson, 2017; Veettil et al., 2017). This is evident in the regression analysis, when the El Niños are removed, the regression improves noticeably and variance testing to evaluate the mean of each variable during these different climatic conditions. Considering the likely continuation of the out of equilibrium state, projections continuing along the linear decline of the SCA and rise of the ELA indicate the possible disappearance of the QIC by 2090 (Fig. S5). Further, with increasing ice loss, there is potential for an uneven ice surface with standing water to change the albedo, and thus affect the QIC's mass balance, enhancing its decline (Naegeli & Huss, 2017; Wang et al., 2015). As the ice continues to retreat, an uneven ice surface, future El Niños, and anthropogenic warming will likely exacerbate the process, pushing its demise closer to the present than expected.

https://doi.org/10.5194/egusphere-2024-676
Preprint. Discussion started: 18 March 2024

5 Conclusion

We automate the process of satellite-based collection of yearly QIC parameters important for mass balance assessment and assess the ice cap's short-term fluctuations to local climate forcings, including temperature fluctuations and El Nino events. We observe and record decadal-scale change and interannual variability with staggering loss over the last four decades. In the height of the wet season, the ONI index is the determining factor for the SCA's end of dry season condition, but as anthropogenic warming continues to overwhelm natural climatic signals the entire SCA continues to rapidly decline. Continued monitoring of the QIC will be vital, as the potential for surface processes and future El Niños to accelerate the ice loss rises with continued warming. The implications for the QIC's future points towards water scarcity for the local population, creating uncharted difficulties alongside the lessening of a water source, especially seasonally (Veettil et al., 2017; Vuille et al., 2018).With ongoing warming, we expect to see continued shrinkage of both the SCA and the entire QIC in the coming decades.

Code and Data Availability

All comprehensive calculated QIC results from this study are provided within the supplementary information, detailed in Table S2. Annual SCA shapefile data and DEM bin distribution initially calculated within GEE is available at the following repository at https://doi.org/10.5281/zenodo.10694300. A sample code for preprocessing and processing Landsat 8 images is available at the following url: https://code.earthengine.google.com/72e85af2cc7c2e10482a939f7dd1cfe6?noload=true.

Author Contribution

K.A.L. designed the study, developed the code, collected the snow cover data, and completed the analysis of the data and accompanying climate variables. K.A.L. and L.J.L wrote the manuscript. K.A.L., L.J.L, L.G.T., and B.G.M. contributed to the discussion of the results, editing, and revision of the manuscript.

Competing Interests

The authors declare that they have no conflict of interest.

Acknowledgments

This research was supported by the Heising-Simons Foundation and Volo Foundation for both past field data used as reference and in support of the current project. We would like to thank the National Science Foundation (NSF) for graduate student support under Award #1805819. Additionally, we thank Rainey Aberle for providing guidance regarding ELA calculations and Shelby Turner for insights into their climate projections in the Peruvian Andes. This is Byrd Polar and Climate Research Center contribution No. 1630.

https://doi.org/10.5194/egusphere-2024-676
Preprint. Discussion started: 18 March 2024

References

Benn, D. I., & Lehmkuhl, F. (2000). Mass balance and equilibrium-line altitudes of glaciers in high-mountain environments. *Quaternary International*, *65*, 15–29.

Bradley, R. S., Keimig, F. T., Diaz, H. F., & Hardy, D. R. (2009). Recent changes in freezing level heights in the Tropics with implications for the deglacierization of high mountain regions. *Geophysical Research Letters*, *36*(17), 2009GL037712. https://doi.org/10.1029/2009GL037712

Bradley, R. S., Vuille, M., Diaz, H. F., & Vergara, W. (2006). Threats to water supplies in the tropical Andes. *Science*, *312*(5781), 1755–1756.

Braun, M. H., Malz, P., Sommer, C., Farías-Barahona, D., Sauter, T., Casassa, G., Soruco, A., Skvarca, P., & Seehaus, T. C. (2019). Constraining glacier elevation and mass changes in South America. *Nature Climate Change*, *9*(2), 130–136.

Brecher, H. H., & Thompson, L. G. (1993). *Measurement of the Retreat of Qori kalis Glacier in the Tropical Andes of Peru by Terrestrial Photogrammetry*. 6.

Casimiro, W.S.L., Labat, D., Ronchail, J., Espinoza, J. C., & Guyot, J. L. (2013). Trends in rainfall and temperature in the Peruvian Amazon–Andes basin over the last 40 years (1965–2007). *Hydrological Processes*, *27*(20), 2944–2957.

Dozier, J. (1989). Spectral signature of alpine snow cover from the Landsat Thematic Mapper. *Remote Sensing of Environment*, *28*, 9–22.

Fang, H., Baiping, Z., Yonghui, Y., Yunhai, Z., & Yu, P. (2011). Mass Elevation Effect and Its Contribution to the Altitude of Snowline in the Tibetan Plateau and Surrounding Areas. *Arctic, Antarctic, and Alpine Research*, *43*(2), 207–212. https://doi.org/10.1657/1938-4246-43.2.207

Favier, V., Wagnon, P., & Ribstein, P. (2004). Glaciers of the outer and inner tropics: A different behaviour but a common response to climatic forcing. *Geophysical Research Letters*, *31*(16).

Gaddam, V. K., Boddapati, R., Kumar, T., Kulkarni, A. V., & Bjornsson, H. (2022). Application of "OTSU"—An image segmentation method for differentiation of snow and ice regions of glaciers and assessment of mass budget in Chandra basin, Western Himalaya using Remote Sensing and GIS techniques. *Environmental Monitoring and Assessment*, *194*(5), 337. https://doi.org/10.1007/s10661-022-09945-2

Ge, H., Lu, D., He, S., Xu, A., Zhou, G., & Du, H. (2008). Pixel-based Minnaert Correction Method for Reducing Topographic Effects on a Landsat 7 ETM+ Image. *Photogrammetric Engineering & Remote Sensing*, *74*(11), 1343–1350. https://doi.org/10.14358/PERS.74.11.1343

Hall, D. K., & Riggs, G. A. (2007). Accuracy assessment of the MODIS snow products. *Hydrological Processes: An International Journal*, *21*(12), 1534–1547.

Hanshaw, M. N., & Bookhagen, B. (2014a). Glacial areas, lake areas, and snow lines from 1975 to 2012: Status of the Cordillera Vilcanota, including the Quelccaya Ice Cap, northern central Andes, Peru. *The Cryosphere*, *8*(2), 359–376. https://doi.org/10.5194/tc-8-359-2014

Hanshaw, M. N., & Bookhagen, B. (2014b). Glacial areas, lake areas, and snow lines from 1975 to 2012: Status of the Cordillera Vilcanota, including the Quelccaya Ice Cap, northern central Andes, Peru. *The Cryosphere*, *8*(2), Article 2. https://doi.org/10.5194/tc-8-359-2014

Hu, Z., Dietz, A., Zhao, A., Uereyen, S., Zhang, H., Wang, M., Mederer, P., & Kuenzer, C. (2020). Snow Moving to Higher Elevations: Analyzing Three Decades of Snowline Dynamics in the Alps. *Geophysical Research Letters*, *47*(12), e2019GL085742. https://doi.org/10.1029/2019GL085742

Hugonnet, R., McNabb, R., Berthier, E., Menounos, B., Nuth, C., Girod, L., Farinotti, D., Huss, M., Dussaillant, I., Brun, F., & Kääb, A. (2021). Accelerated global glacier mass loss in the early twenty-first century. *Nature*, *592*(7856), 726–731. https://doi.org/10.1038/s41586-021-03436-z

Kaser, G., & Osmaston, H. (2002). *Tropical glaciers*. Cambridge University Press.

Klein, A. G., & Isacks, B. L. (1999). Spectral mixture analysis of Landsat thematic mapper images applied to the detection of the transient snowline on tropical Andean glaciers. *Global and Planetary Change*, *22*(1–4), 139–154. https://doi.org/10.1016/S0921-8181(99)00032-6

https://doi.org/10.5194/egusphere-2024-676
Preprint. Discussion started: 18 March 2024

Lagos, P., Silva, Y., Nickl, E., & Mosquera, K. (2008). El Niño–related precipitation variability in Perú. *Advances in Geosciences*, *14*, 231–237.

Li, X., Wang, N., & Wu, Y. (2022). Automated Glacier Snow Line Altitude Calculation Method Using Landsat Series Images in the Google Earth Engine Platform. *Remote Sensing*, *14*(10), 2377. https://doi.org/10.3390/rs14102377

Liu, C., Li, Z., Zhang, P., Tian, B., Zhou, J., & Chen, Q. (2021). Variability of the snowline altitude in the eastern Tibetan Plateau from 1995 to 2016 using Google Earth Engine. *Journal of Applied Remote Sensing*, *15*(04). https://doi.org/10.1117/1.JRS.15.048505

Lopez, H., Lee, S.-K., Kim, D., Wittenberg, A. T., & Yeh, S.-W. (2022). Projections of faster onset and slower decay of El Niño in the 21st century. *Nature Communications*, *13*(1), 1915.

Mark, B. G., Seltzer, G. O., Rodbell, D. T., & Goodman, A. Y. (2002). Rates of Deglaciation during the Last Glaciation and Holocene in the Cordillera Vilcanota-Quelccaya Ice Cap Region, Southeastern Perú. *Quaternary Research*, *57*(3), Article 3. https://doi.org/10.1006/qres.2002.2320

Martín-Ortega, P., García-Montero, L. G., & Sibelet, N. (2020). Temporal patterns in illumination conditions and its effect on vegetation indices using Landsat on Google Earth Engine. *Remote Sensing*, *12*(2), 211.

Meier, M. F. (1962). Proposed definitions for glacier mass budget terms. *Journal of Glaciology*, *4*(33), 252–263.

Naegeli, K., & Huss, M. (2017). Sensitivity of mountain glacier mass balance to changes in bare-ice albedo. *Annals of Glaciology*, *58*(75pt2), 119–129.

Pepin. (2015). Elevation-dependent warming in mountain regions of the world. *Nature Climate Change*, *5*(5), 424–430.

Racoviteanu, A. E., Rittger, K., & Armstrong, R. (2019). An Automated Approach for Estimating Snowline Altitudes in the Karakoram and Eastern Himalaya From Remote Sensing. *Frontiers in Earth Science*, *7*, 220. https://doi.org/10.3389/feart.2019.00220

Rounce, D. R., Hock, R., Maussion, F., Hugonnet, R., Kochtitzky, W., Huss, M., Berthier, E., Brinkerhoff, D., Compagno, L., & Copland, L. (2023). Global glacier change in the 21st century: Every increase in temperature matters. *Science*, *379*(6627), 78–83.

Sankey, T., Donald, J., McVay, J., Ashley, M., O'Donnell, F., Lopez, S. M., & Springer, A. (2015). Multi-scale analysis of snow dynamics at the southern margin of the North American continental snow distribution. *Remote Sensing of Environment*, *169*, 307–319.

Schauwecker, S., Rohrer, M., Acuña, D., Cochachin, A., Dávila, L., Frey, H., Giráldez, C., Gómez, J., Huggel, C., Jacques-Coper, M., Loarte, E., Salzmann, N., & Vuille, M. (2014). Climate trends and glacier retreat in the Cordillera Blanca, Peru, revisited. *Global and Planetary Change*, *119*, 85–97. https://doi.org/10.1016/j.gloplacha.2014.05.005

Seehaus, T., Malz, P., Sommer, C., Soruco, A., Rabatel, A., & Braun, M. (2020). Mass balance and area changes of glaciers in the Cordillera Real and Tres Cruces, Bolivia, between 2000 and 2016. *Journal of Glaciology*, *66*(255), 124–136.

Thompson, L. G. (2000). Ice core evidence for climate change in the Tropics: Implications for our future. *Quaternary Science Reviews*, *19*(1–5), Article 1–5. https://doi.org/10.1016/S0277-3791(99)00052-9

Thompson, L. G. (2017). Past, present, and future of glacier archives from the world's highest mountains. *Proceedings of the American Philosophical Society*, *161*(3), 226–243.

Thompson, L. G., Davis, M. E., Mosley-Thompson, E., Beaudon, E., Porter, S. E., Kutuzov, S., Lin, P. -N., Mikhalenko, V. N., & Mountain, K. R. (2017). Impacts of Recent Warming and the 2015/2016 El Niño on Tropical Peruvian Ice Fields. *Journal of Geophysical Research: Atmospheres*, *122*(23). https://doi.org/10.1002/2017JD026592

Thompson, L. G., Davis, M. E., Mosley-Thompson, E., Porter, S. E., Corrales, G. V., Shuman, C. A., & Tucker, C. J. (2021). The impacts of warming on rapidly retreating high-altitude, low-latitude glaciers and ice core-derived climate records. *Global and Planetary Change*, *203*, 103538. https://doi.org/10.1016/j.gloplacha.2021.103538

Thompson, L. G., Mosley-Thompson, E., Bolzan, J. F., & Koci, B. R. (1985). A 1500-Year Record of Tropical Precipitation in Ice Cores from the Quelccaya Ice Cap, Peru. *Science*, *229*(4717), Article 4717. https://doi.org/10.1126/science.229.4717.971

Thompson, L. G., Mosley-Thompson, E., Davis, M. E., & Brecher, H. H. (2011). Tropical glaciers, recorders and indicators of climate change, are disappearing globally. *Annals of Glaciology*, *52*(59), 23–34. https://doi.org/10.3189/172756411799096231

https://doi.org/10.5194/egusphere-2024-676
Preprint. Discussion started: 18 March 2024

Thompson, L. G., Mosley-Thompson, E., Davis, M. E., Zagorodnov, V. S., Howat, I. M., Mikhalenko, V. N., & Lin, P.-N. (2013). Annually Resolved Ice Core Records of Tropical Climate Variability over the Past ~1800 Years. *Science*, *340*(6135), Article 6135. https://doi.org/10.1126/science.1234210

Veettil, B. K., Wang, S., Florêncio de Souza, S., Bremer, U. F., & Simões, J. C. (2017). Glacier monitoring and glacier-climate interactions in the tropical Andes: A review. *Journal of South American Earth Sciences*, *77*, 218–246. https://doi.org/10.1016/j.jsames.2017.04.009

Vuille, M., Bradley, R. S., & Keimig, F. (2000). Interannual climate variability in the Central Andes and its relation to tropical Pacific and Atlantic forcing. *Journal of Geophysical Research: Atmospheres*, *105*(D10), 12447–12460. https://doi.org/10.1029/2000JD900134

Vuille, M., Carey, M., Huggel, C., Buytaert, W., Rabatel, A., Jacobsen, D., Soruco, A., Villacis, M., Yarleque, C., Elison Timm, O., Condom, T., Salzmann, N., & Sicart, J.-E. (2018). Rapid decline of snow and ice in the tropical Andes – Impacts, uncertainties and challenges ahead. *Earth-Science Reviews*, *176*, 195–213. https://doi.org/10.1016/j.earscirev.2017.09.019

Vuille, M., Franquist, E., Garreaud, R., Lavado Casimiro, W. S., & Cáceres, B. (2015). Impact of the global warming hiatus on Andean temperature. *Journal of Geophysical Research: Atmospheres*, *120*(9), Article 9.

Vuille, M., Kaser, G., & Juen, I. (2008). Glacier mass balance variability in the Cordillera Blanca, Peru and its relationship with climate and the large-scale circulation. *Global and Planetary Change*, *62*(1–2), 14–28. https://doi.org/10.1016/j.gloplacha.2007.11.003

Wang, W., Xiang, Y., Gao, Y., Lu, A., & Yao, T. (2015). Rapid expansion of glacial lakes caused by climate and glacier retreat in the Central Himalayas. *Hydrological Processes*, *29*(6), 859–874.

Yarleque, C., Vuille, M., Hardy, D. R., Timm, O. E., De la Cruz, J., Ramos, H., & Rabatel, A. (2018). Projections of the future disappearance of the Quelccaya Ice Cap in the Central Andes. *Scientific Reports*, *8*(1), 1–11.

Zekollari, H., Huss, M., & Farinotti, D. (2020). On the imbalance and response time of glaciers in the European Alps. *Geophysical Research Letters*, *47*(2), e2019GL085578.